H. F. (1985) *Science 229*, 941–945.
Parker, C. A. (1968) *Photoluminescence of Solutions*, p 222, American Elsevier, Amsterdam.
Pawagi, A. B., & Deber, C. M. (1990) *Biochemistry 29*, 950–955.
Pinkofsky, H. B., Rampal, A. L., Cowden, M. A., & Jung, C. Y. (1978) *J. Biol. Chem. 253*, 4930–4937.
Rampal, A. L., & Jung, C. Y. (1987) *Biochim. Biophys. Acta 896*, 287–294.
Rampal, A. L., Jung, E. K. Y., Chin, J. J., Deziel, M. R., Pinkofsky, H. B., & Jung, C. Y. (1986) *Biochim. Biophys. Acta 859*, 135–142.
Shanahan, M. F., Morris, D. P., & Edwards, B. M. (1987) *J. Biol. Chem. 262*, 5978–5984.
Sogin, D. C., & Hinkle, P. C. (1978) *J. Supramol. Struct. 8*, 447–453.
Stein, W. D. (1986) in *Transport and Diffusion Across Cell Membranes*, p 355, Academic Press, Inc., Orlando, FL.
Stryer, L. (1975) in *Biochemistry*, p 86, W. H. Freeman, San Francisco.
Tanford, C. (1982) *Proc. Natl. Acad. Sci. U.S.A. 79*, 2882–2884.
Weber, G., & Teal, F. W. J. (1965) *Proteins (2nd Ed.) 3*, 445.
Wheeler, T. J., & Hinkle, P. C. (1981) *J. Biol. Chem. 256*, 8907–8914.
White, A., Handler, P., Smith, E. L., Hill, R. L., & Lehman, I. R. (1978) in *Principles of Biochemistry*, 6th ed., p 107, McGraw-Hill, New York.

Structural Analysis of the Operator Binding Domain of Tn10-Encoded Tet Repressor: A Time-Resolved Fluorescence and Anisotropy Study

Marie Chabbert,[‡] Wolfgang Hillen,[§] Dieter Hansen,[§,∥] Masayuki Takahashi,[⊥] and Jean-Alain Bousquet*[,‡]

CNRS UA 491, Laboratoire de Physique, Faculté de Pharmacie de Strasbourg, BP 24, F-67401 Illkirch, France, Groupe de Cancérogénèse et de Mutagénèse Moléculaire et Structurale, IBMC du CNRS et Université Louis Pasteur, 15 rue René Descartes, F-67084 Strasbourg, France, and Lehrstuhl für Mikrobiologie, Institut für Mikrobiologie und Biochemie der Friedrich-Alexander Universität, Erlangen-Nürnberg, Staudtstrasse 5, G-8520 Erlangen, Federal Republic of Germany

Received May 31, 1991; Revised Manuscript Received November 22, 1991

ABSTRACT: An engineered Tn10-encoded Tet repressor, bearing a single Trp residue at position 43, in the putative α-helix–turn–α-helix motif of the operator binding domain, was studied by time-resolved fluorescence and anisotropy. Fluorescence intensity decay data suggested the existence of two classes of Trp-43, defined by different lifetimes. Analysis of anisotropy data were consistent with a model in which each class was defined by a different lifetime, rotational correlation time, and fluorescence emission maximum. The long-lifetime class had a red-shifted spectrum, similar to that of tryptophan zwitterion in water, and a short rotational correlation time. In contrast, the spectrum of the short-lifetime class was blue-shifted 10 nm compared to that of the long-lifetime class. Its correlation time was similar to that of the protein, which showed that Trp in this class was entirely constrained. Trp in this latter class could not be quenched by iodide, whereas most of the long-lifetime class was easily accessible. Presence of disruptive agents, such as 1 M GuCl or 3 M KCl, did not alter markedly the lifetimes but increased the weight of the short-lifetime component. In the same time, the rotational correlation time of this component was dramatically reduced. Taken together, our data suggest that the long-lifetime class could correspond to the tryptophan residues exposed to solvent whereas the short-lifetime class would correspond to the tryptophan residues embedded inside the hydrophobic core holding the helix–turn–helix motif. Destabilization of hydrophobic interactions would lead to an increase in the weight of the latter class for entropic reasons. Analysis of the fluorescence parameters of Trp-43 could provide structural information on the operator binding domain of Tet repressor.

Regulation of gene expression in procaryotes is often mediated by proteins which recognize DNA sequence specifically (Pabo & Sauer, 1984). The ability of many regulatory proteins to recognize the respective target DNA depends on the presence, e.g., Trp repressor (Gunsalus & Yanofsky, 1980), or the absence of effector molecules, e.g., Lac repressor (Miller & Reznikoff, 1980). X-ray analyses of the crystal structure of several repressors provide keys to the molecular basis of sequence specificity in DNA binding proteins. These data reveal that an α-helix–turn–α-helix structural motif is a common feature for sequence-specific DNA recognition among procaryotic DNA binding proteins (Pabo & Sauer, 1984). This α-helix–turn–α-helix motif makes sequence-specific contacts in the major groove of B-DNA. In this model, sequence specificity is achieved by interactions of amino acid side chains with solvent-exposed functions of the base pairs (Pabo & Sauer, 1984; Harrison & Aggarval, 1990).

Tet repressor controls transcription of the Tn10-encoded *tet* genes conferring resistance to tetracycline in Gram-negative bacteria (Beck et al., 1982; Bertrand et al., 1983; Hillen et al., 1984). This control is negatively regulated by the antibiotic tetracycline (Yang et al., 1976), which functions as an inducer (Hillen et al., 1983, 1984). Tet repressor has been purified and characterized (Hillen et al., 1982; Oehmichen et al., 1984) and its sequence has been determined (Postle et al., 1984). The comparison of Tet repressor with other repressor sequences (Pabo & Sauer, 1984) and the positions of trans-dominant mutations with reduced operator binding affinity (Isackson

[‡] Faculté de Pharmacie de Strasbourg.
[§] Institut für Mikrobiologie und Biochemie der Friedrich-Alexander Universität.
[∥] Present address: Henkel KGaA, TFB Biotechnologie, Henkelst. 67, G-4000 Düsseldorf, FRG.
[⊥] IMBC du CNRS et Université Louis Pasteur.

0006-2960/92/0431-1951$03.00/0

& Bertrand, 1985) strongly suggest that an α-helix–turn–α-helix motif is involved in sequence-specific DNA binding.

Comparison of the repressor gene sequences from each of the five classes of tetracycline resistance genes from Gram-negative bacteria (Mendez et al., 1980; Tovar et al., 1988) shows that the repressor protein from each class contains only two tryptophan residues at conserved positions (Unger et al., 1984). This suggests that these residues are important for repressor structure and/or function. In Tn10-encoded Tet repressor, these residues are located at position 43 and 75. Tet repressor mutants with either one or both of the tryptophans replaced by a phenylalanine have been engineered (Hansen & Hillen, 1987). These mutated proteins maintain the ability to bind *tet* operator DNA and tetracycline, albeit with altered affinity, and to act as a repressor (Hansen & Hillen, 1987; Hansen et al., 1987). A sequence-specific contact between Trp-43 and *tet* operator DNA has been suggested by fluorescence spectroscopy of these mutants and quantitative binding analysis of the respective complexes (Hansen & Hillen, 1987). As a matter of fact, Trp-43 is located in α-helix 3 of Tet repressor, part of the proposed α-helix–turn–α-helix motif.

In this report, we summarize the results of a fluorescence analysis of F75 TetR, an engineered Tet repressor containing a single Trp residue at position 43 (Hansen & Hillen, 1987). Our data are consistent with the existence of an equilibrium between two classes of Trp-43. These classes are defined by different lifetimes, maximum emission wavelengths, correlation rotational times, and quencher accessibilities. These parameters are altered by the presence of disruptive agents and might provide information on the conformation of the α-helix–turn–α-helix motif.

Materials and Methods

Chemicals. All chemicals were of reagent grade or better. High-purity sodium chloride was purchased from Prolabo; Tris was from Serva. Potassium iodide was from Merck and guanidine hydrochloride from Sigma. Ultrapure water (MilliQ instrument from Millipore Corp.) was used throughout the experiments. The dimer protein concentration usually ranged around 3 μM.

All experiments were performed in 10 mM Tris-HCl, pH 8.0, 100 mM NaCl, 5 mM $MgCl_2$, and either 1 mM DTT or 10 mM β-mercaptoethanol. The addition of other chemicals in the buffer will be noted specifically. The pH was adjusted to 8.00 ± 0.05, after correction for the temperature dependence of the pK_a of the Tris buffer. The temperature was controlled at 20 ± 1 °C.

F75 TetR Preparation. The mutated F75 Tet repressor differs from the wild type by the replacement of Trp-75 by Phe. After the preparation carried out as described in detail elsewhere (Hansen & Hillen, 1987), a further purification step using the FPLC system from Pharmacia was added to remove the fluorescence contamination previously observed (Hansen & Hillen, 1987). The sample was loaded on a MonoQ column equilibrated in 10 mM Tris-HCl, pH 8.0, and 0.1 mM DTT and eluted with a NaCl linear gradient from 10 mM Tris-HCl, pH 8.0, and 0.1 mM DTT to 10 mM Tris-HCl, pH 8.0, 0.1 mM DTT, and 0.5 M NaCl. The main peak, which eluted at 0.35 M NaCl, was collected and dialyzed against 0.1 M NaCl. It was free from fluorescent contamination, as controlled by using the double-mutant repressor, F43F75 TetR, whose two tryptophan residues were changed to Phe.

The protein was precipitated by addition of ammonium sulfate until 60% saturation was reached and stocked at 4 °C in 10 mM Tris-HCl, pH 8.0, 100 mM NaCl, 2 mM DTT, 1 mM EDTA, and 60% ammonium sulfate. Before measurements, the protein solution was extensively dialyzed against 10 mM Tris-HCl, pH 8.0, 100 mM NaCl, and either 1 mM DTT or 10 mM β-mercaptoethanol. The concentration of F75 TetR was determined by absorption, using an extinction coefficient of 7000 at 280 nm. This value was determined by measuring the absorption of a protein solution in 10 mM ammonium carbonate and, then, the concentration of the same solution by amino acid analysis.

Spectroscopic Methods. UV absorption spectra were recorded on a Cary 219 spectrophotometer. Steady-state fluorescence measurements were performed with a MPF 66 spectrofluorometer (Perkin-Elmer). The excitation wavelength was set at 295 nm to avoid contribution from tyrosine residues. The quantum yields were determined relative to that of tryptophan zwitterion at pH 7.0 (0.14).

The iodide quenching measurements were carried out by adding aliquots of a concentrated stock solution of iodide (6 M) to the protein solution. For each iodide concentration, the total fluorescence intensity was determined from the area under the spectrum and was corrected for the buffer baseline, the dilution effect, and the ionic strength effect.

Fluorescence lifetime measurements were performed with the pulse fluorometry technique. A complete description of the device has been reported elsewhere (Montoro et al., 1988). Briefly, a mode-locked Argon laser (SpectraPhysics) synchronously pumped a rhodamine 6G dye laser (SpectraPhysics). The pulse repetition rate of the dye laser was controlled by a cavity dumper and set at 80 kHz. Output pulses (full width at half maximum 20 ps), tuned at 590 nm, were upconverted with a frequency doubler employing a temperature-tuned KDP crystal.

The emission was detected by using the single-photon counting method with a Phillips XP 2020 photomultiplier, at a right angle to the excitation beam, through a polarizer set at 54.7° from the excitation beam polarization to eliminate artifacts due to the rotation of the protein molecule. The emission wavelength was selected with a 8-nm monochromator (Jobin-Yvon H10). A Schott WG 320 filter was added in front of the monochromator to eliminate most of the light scattering. To take into account the wavelength dependence of the photomultiplier, the instrument response functions (full width at half maximum around 500 ps) were determined by collecting the emission from a *p*-terphenyl solution in a cyclohexane–CCl_4 mixture (4:3) at the same wavelength as the decay studied. The fluorescence lifetime of *p*-terphenyl in this solution was < 20 ps, and, thus, its observed decay was indistinguishable from the response function (Kolber & Barkley, 1986).

The data were recorded on a multichannel analyzer (Ortec 7100). For both the sample decay and the response function, the couning was stopped when the peak channel reached 10^4 counts. The calibration was 108 ps/channel. The decay data were transmitted to an IBM 3090 computer and analyzed as sums of exponentials:

$$I(t,\lambda) = \sum_i \alpha_i(\lambda) e^{-t/\tau i(\lambda)} \quad (1)$$

with

$$\sum_i \alpha_i(\lambda) = 1$$

by an iterative reconvolution procedure based on the Marquardt algorithm. The number of exponentials was progressively increased until the fit did not improve. The adequacy of the fit was judged by the value of reduced χ^2 and by visual inspection of the autocorrelation functions and of the weighted residuals, defined as the difference between the calculated and

Table I: Analysis of Typical Fluorescence Decays of F75 TetR Using an Increasing Number of Exponential Components[a]

λ (nm)	n	τ_1 (ns)	F_1	τ_2 (ns)	F_2	τ_3 (ns)	F_3	χ^2
320	1	3.3	1					49
	2	4.4	0.82	0.9	0.18			3.3
	3	4.6	0.79	1.1	0.18	0.07	0.03	1.6
360	1	4.2	1					17
	2	4.9	0.90	1.3	0.10			1.6
	3	4.9	0.90	1.3	0.10	0.09	<0.005	1.5

[a] F_i represents the weight of component i in the total fluorescence intensity. The experiments were carried out as described under Materials and Methods, in 10 mM Tris-HCl, pH 8.0, 100 mM KCl, 5 mM $MgCl_2$, and 1 mM DTT.

experimental decay at each channel divided by the square root of the experimental decay value.

Decay-associated spectra (DAS) were calculated from the steady-state fluorescence spectra and the multiexponential analysis of the decay data. The fluorescence associated with the component i at the wavelength λ was calculated from the formula (Donzel et al., 1974)

$$F_i(\lambda) = F(\lambda)\alpha_i(\lambda)\tau_i(\lambda)/\sum_j \alpha_j(\lambda)\tau_j(\lambda) \quad (2)$$

Anisotropy Measurements. The steady-state anisotropy measurements were carried out on a SLM 8000 spectrofluorometer with the excitation wavelength set at 295 nm, by measuring alternatively the emission light parallel and perpendicular to the excitation beam. The data were corrected from Rayleigh and Raman scattering and buffer contribution.

Anisotropy associated spectra were calculated from the corrected anisotropy data by using the formula

$$r(\lambda) = \sum_i I_i(\lambda) r_i \quad (3)$$

with

$$\sum_i I_i(\lambda) = 1$$

where r_i represents the intrinsic anisotropy of species i and $I_i(\lambda)$ the relative weight of species i in the fluorescence intensity at the wavelength λ. The intrinsic anisotropies r_i were calculated from the anisotropies measured at 350 and 400 nm.

The time-resolved anisotropy measurements were carried out with the same device as the decay experiments. The polarization of the excitation beam was alternated by using a home-built device. The polarization of the emission was vertical. This procedure avoided polarization bias. The vertical and horizontal decays, $I_\parallel(t)$ and $I_\perp(t)$, were alternatively recorded during 30 s each. The counting was stopped when the total fluorescence intensity decay, defined as $I_t(t) = I_\parallel(t) + 2I_\perp(t)$, reached 10^5 peak channel counts. The anisotropy decay is defined as

$$r(t) = [i_\parallel(t) - i_\perp(t)]/[i_\parallel(t) + 2i_\perp(t)] \quad (4)$$

where $i_\parallel(t)$ and $i_\perp(t)$ are the true decay functions. After the analysis of the total fluorescence decay as the sum of exponentials, the individual vertical and horizontal decays were fit simultaneously with optimization of the anisotropy decay parameters (Cross & Fleming, 1984). The anisotropy decay functions were fit to sums of exponential terms. An adequate fit was determined by evaluating χ^2 and by examining plots of the residuals.

Results

Decay-Associated Spectra. Table I reports the analysis of F75 TetR fluorescence decay using an increasing number of exponential terms at two wavelengths, typical of the decay behavior on the blue edge (λ < 340 nm) and on the red edge (λ ≥ 340 nm) of the spectrum. At wavelengths equal to or greater than 340 nm (e.g., 360 nm), the fluorescence intensity decay could be described adequately by a biexponential function. Obviously, the decay was nonexponential. The addition of a second component in the fit decreased dramatically the reduced χ^2 from 17 to 1.6. The addition of a third component increased χ^2 only marginally. The corresponding decay is reported in Figure 1, along with the plots of the weighted residuals using one, two, and three components in the fitting procedure. The presence of a third component did not improve the accuracy of the fit. On the blue edge of the spectrum, however, the presence of a subnanosecond component with a lifetime < 100 ps improved the fit (Table I). This component represented only a few percent of the fluorescence intensity, which did not allow quantitative measurements. It was probably due to contamination of the decay by Rayleigh and Raman scattering as its weight increased significantly at 330 nm, for which Raman scattering was expected (not shown). In any case, most of the fluorescence decay could be described by two components and the additional subnanosecond component did not affect significantly the observed time-resolved spectra. Consequently, at these wavelengths, we took into account only the two main components obtained by using a three-component analysis, with their preexponential terms normalized to have a sum equal to 1.

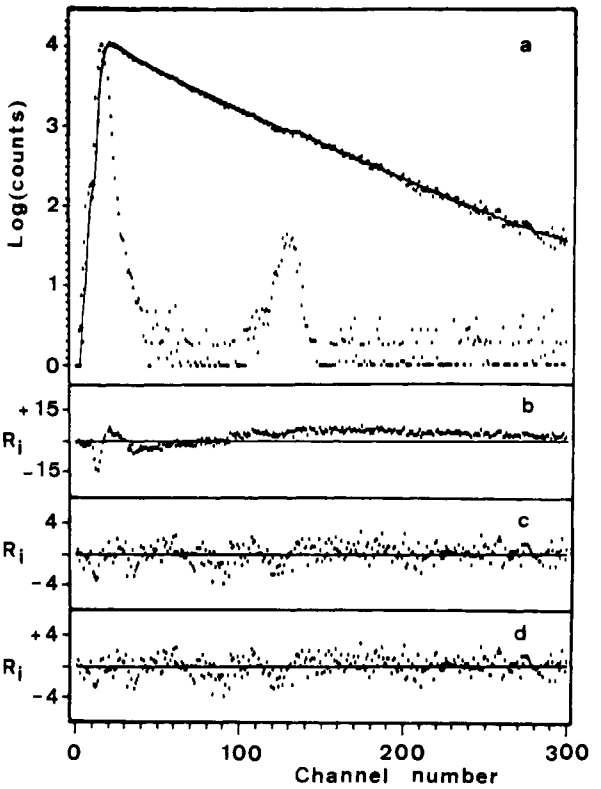

FIGURE 1: Typical fluorescence decay of F75 TetR at 360 nm. The experiments were carried out as outlined under Materials and Methods. The solid line in panel a is the computed curve reconvolved by using the optimal biexponential fit. The weighted residuals, R_i, are plotted for the optimal monoexponential (b), biexponential (c), and triexponential (d) fits. The corresponding decay parameters are reported in Table I. The calibration was 108 ps/channel.

Figure 2 summarizes the parameters describing the fluorescence decay throughout the spectrum. The two lifetimes were roughly independent of the wavelength (Figure 2a). The long lifetime, τ_1, slightly increased with the emission wavelength to plateau at 5.0 ± 0.2 ns above 330 nm, whereas the short lifetime, τ_2, averaged at 1.3 ± 0.2 ns. The relative

Table II: Spectra-Associated Parameters of F75 TetR under Various Experimental Conditions[a]

	λ_{max} (nm)	Φ	τ_1 (ns)	α_1	τ_2 (ns)	α_2	$\bar{\tau}$ (ns)	θ_1 (ns)	θ_2 (ns)
buffer T	351	0.14	5.0	0.65	1.3	0.35	3.7	1.9	16
+0.2 M KI	347	0.07	2.4	0.58	1.3	0.42	1.9	1.9	16
+1 M GuCl	342	0.09	4.8	0.34	1.4	0.66	2.6	2.0	4
+6 M GuCl	352	0.06	4.2	0.24	1.2	0.76	1.9	1.0	0.7
+3 M KCl	347	0.11	5.0	0.46	1.4	0.54	3.1	2.1	12

[a] The experiments have been carried out as described under Materials and Methods, in 10 mM Tris-HCl, pH 8.0, 100 mM KCl, 5 mM $MgCl_2$, and either 1 mM DTT or 10 mM β-mercaptoethanol (buffer T). The excitation wavelength was set at 295 nm and the emission one at 350 nm. The dimer protein concentration was around 3×10^{-6} M. λ_{max} represents the emission maximum wavelength and Φ the quantum yield. τ_i and α_i are the lifetime and amplitude, respectively, of component i; θ_i is its correlation rotational time calculated from eq 8 as described in the text. The average lifetime is defined as $\bar{\tau} = \Sigma_i \alpha_i \tau_i$.

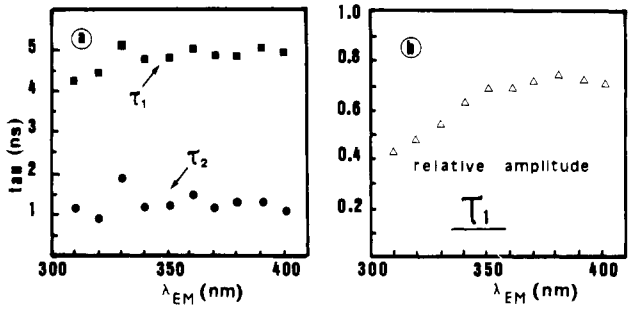

FIGURE 2: Wavelength dependence of the fluorescence decay parameters of F75 TetR. The decay times, τ_1 (squares) and τ_2 (circles) (a) and the relative amplitude (triangles) of the 5-ns component (component 1) (b) are plotted versus the fluorescence emission wavelength; the excitation wavelength is 295 nm. At wavelengths $\leq$ 330 nm, the data plotted correspond to the two main components of the decay fit with three exponentials (see text).

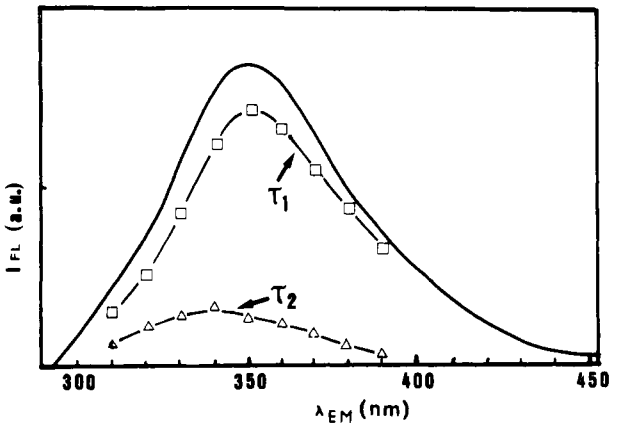

FIGURE 3: Resolution of F75 TetR fluorescence emission spectrum into two spectra associated with the 5.0-ns (open squares) and 1.3-ns (open triangles) components. The solid line represents the steady-state fluorescence spectrum of F75 TetR under the same experimental conditions.

amplitude of the long component, α_1, increased markedly from 0.44 on the blue edge of the spectrum to 0.72 on the red edge (Figure 2b). This corresponds to an increase in its weight from 74% to 90%. From these parameters and the steady-state spectrum, we could calculate the spectra associated with each component of the decay (DAS), as described in Materials and Methods (Figure 3). The steady-state spectrum of Trp-43 had an emission maximum at 351 nm, very similar to the value of 352 nm for the emission maximum of Trp zwitterion in water, as determined with our experimental device. This value is closely related to that previously reported (Hansen et al., 1987), taking into account a systematic difference between the two devices.

The fluorescence emission of F75 TetR was dominated by that of the long-lifetime component, whose emission maximum was around 350 nm. The spectrum of the short-lifetime component was blue-shifted 10 nm as compared to that of class 1 and participated to about 15% to the total fluorescence intensity.

The wavelength independence of the decay times that describe the decay suggests that it may be possible to ascribe a physical meaning to the mathematically resolved individual decay components and that two classes for this tryptophan residue, defined by different lifetimes, exist (see Discussion). On the assumption that these classes do not interconvert during the fluorescence lifetime, the decay times determined experimentally correspond to the lifetimes of the individual components and the spectra determined from eq 2 correspond to those of each class of Trp (Donzel et al., 1974). With the additional hypothesis that the two classes have identical radiative decay rates and molar extinction coefficients, the ratio a_1/a_2 of the relative ground-state concentrations of the two classes can be estimated from the formula (Donzel et al., 1974)

$$a_1/a_2 = (S_1/S_2)(\tau_2/\tau_1) \quad (5)$$

where S_i represents the area under the spectrum i.

Alternatively, this ratio can be estimated from that of the preexponential factors at the isosbestic wavelength of the normalized spectra of the two components, 345 nm (not shown). The ratio of the preexponential factors at 350 nm gives, thus, a quite satisfying approximation of the relative ratio of each class.

Under the previous assumptions, an apparent radiative decay rate k_r can be estimated from the quantum yield Φ of Trp-43 and the decay parameters at 350 nm as

$$\Phi = \sum_i a_i \Phi_i \quad (6)$$

where Φ_i is the quantum yield of species i and a_i its relative molar ratio. This implies

$$\Phi = k_r(\sum_i a_i \tau_i) \quad (7)$$

The quantum yield of Trp-43 is 0.14, very similar to that of Trp in water (Table II). The estimate of k_r, 0.037×10^9 s^{-1}, is significantly lower than the average value of 0.045×10^9 s^{-1} determined for different derivatives of indoles (Ricci, 1970) or that of 0.050 determined for *N*-acetyl-L-tryptophanamide in water (Werner & Forster, 1979). This could be due to perturbation of the electronic state of Trp-43 or to a static quenching of this chromophore. As the study by Ricci (1970) has shown that the radiative decay rates of a large number of indole derivatives in water are very similar, the latter explanation is more likely. This could be related to the vicinity of His-44 as this residue can quench the fluorescence of tryptophan statically (Shinitzky & Goldman, 1967; Pigault & Gérard, 1989). Assuming that k_r for Trp-43 is equal to 0.045×10^9 s^{-1} and that the two classes have the same degree of static quenching, this one would be around 20%.

We have to point out that the initial assumptions of identical radiative decay rates and extinction coefficients for the two

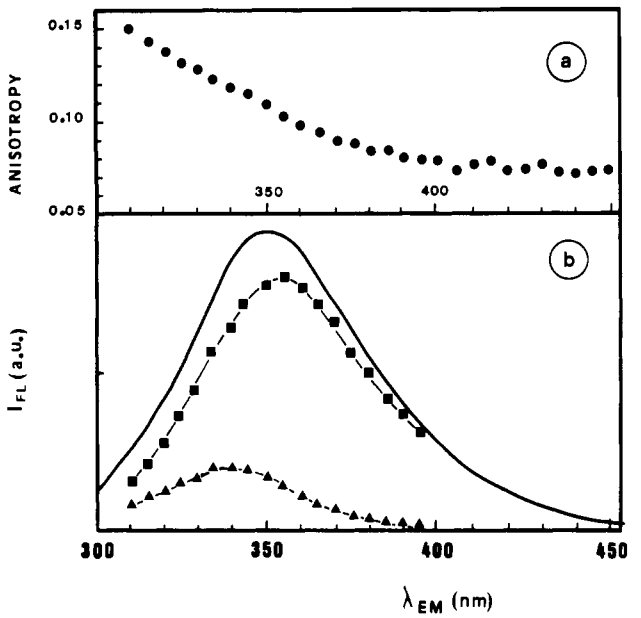

FIGURE 4: (a) Effect of the emission wavelength on the fluorescence anisotropy of native F75 TetR. (b) Resolution of native F75 TetR fluorescence emission spectrum into two spectra associated with the individual anisotropies of class 1 (r_1 = 0.07) (closed squares) and of class 2 (r_2 = 0.25) (closed triangles). The solid line represents the steady-state fluorescence spectrum of F75 TetR under the same experimental conditions.

components cannot be rigorously valid as these parameters depend on the solvent environment (Meech et al., 1983; Chignell & Gratzer, 1968), which is different for the two classes (see below). These assumptions, however, allow an estimate of k_r for the long-lifetime component which dominates the fluorescence emission.

Anisotropy-Associated Spectra. Figure 4a reports the steady-state fluorescence anisotropy of F75 TetR as a function of the emission wavelength. The anisotropy decreased markedly from the blue edge (0.15) to the red edge (0.07) of the spectrum. Taken together with the fluorescence decay data, this suggests that the wavelength dependence of the anisotropy results from a different intrinsic anisotropy r_i for each class of Trp-43. As the long-lifetime component represented around 90% of the fluorescence intensity on the red edge of the spectrum, we made the approximation that the fluorescence anisotropy at wavelengths larger than 400 nm corresponded to that of class 1 (r_1 = 0.075 ± 0.005). The anisotropy of the short-lifetime class (class 2) was determined from the anisotropy at 350 nm, using the relative intensities of the two classes at 350 nm determined by time-resolved fluorescence. This led to r_2 = 0.25 ± 0.01. The anisotropy-associated spectra (AAS) of classes 1 and 2 were then calculated according to eq 3 (Figure 4b). They were strikingly similar to the decay associated spectra (compare Figures 3 and 4b).

To give a qualitative idea of the motion rates involved for a given anisotropy, we analyzed the anisotropy r_i of each class according to the Perrin formula (Lakowicz, 1983):

$$r_0/r_i = 1 + \tau_i/\theta_i \quad (8)$$

where θ_i is the rotational correlation time of Trp in class i and τ_i is its lifetime. The fundamental anisotropy r_0 of Trp-43 was measured at −80 °C in glycerol. Its value was 0.27 at 295 nm, identical to that measured for tryptophan under the same experimental conditions and very similar to that determined for indole in propylene glycol at −58 °C (Valeur & Weber, 1977). This clearly shows that no energy transfer occurs between the two Trp-43 residues of the TetR dimer. The fundamental anisotropy can reasonably be assumed to be identical for the two emitting classes and thus equal to that determined previously. This gave us the so-called rotational correlation times, θ_1 = 1.9 ns for class 1 and θ_2 = 16 ns for class 2 (Table II).

The rotational correlation time of the dimer protein can be estimated from the formula $\theta_p \simeq \eta V_h/kT$, where V_h is the hydrated molecular volume, η is the solvent viscosity, T is the absolute temperature and k is Boltzmann's constant. Empirically, the hydrated molecular volume for a protein is about 1 cm^3 g^{-1}. The molecular weight of TetR dimer is 46 000 (Postle et al., 1984). This led to an estimate for θ_p of 20 ns. The former formula is rigorously valid only for a spherical protein. Neutron scattering studies have evidenced that TetR dimer has an elongated prolate shape (Lederer et al., 1989). The formula can thus give only a rough estimate of the rotational correlation time. However, this supports the inference that the motions of Trp in class 2 are very constrained, whereas Trp in class 1 has an important rotational freedom.

Time-Resolved Fluorescence Anisotropy. Time-resolved anisotropy experiments were carried out at 350 nm as described in Materials and Methods. The anisotropy decay was analyzed as the sum of exponentials and best fitted by the sum of two exponentials with a long rotational correlation time θ_l of 18 ± 2 ns and a short one, θ_s, of 2 ns (not shown).

When several fluorophores are present (or, as here, different species of a fluorophore are in equilibrium), the observed anisotropy decay is a weighted average of the anisotropies attributed to the individual populations. To describe the movement of each species, we used the expression derived by Lipari and Szabo (1980) in a theoretical treatment of fluorescence probes attached to macromolecules. The anisotropy decay of Trp-43 is

$$r(t) = [r_1(t)\alpha_1 e^{-t/\tau_1} + r_2(t)\alpha_2 e^{-t/\tau_2}]/(\alpha_1 e^{-t/\tau_1} + \alpha_2 e^{-t/\tau_2}) \quad (9)$$

with

$$r_i(t) = [(r_0 - r_{\infty i})e^{-t/\theta_{loci}} + r_{\infty i}]e^{-t/\theta_p} \quad (10)$$

where r_0 is the fundamental anisotropy of the chromophore, θ_p is the rotational correlation time of the protein, θ_{loci} is the rotational correlation time of the local motion of class i, and $r_{\infty i}$ is its limiting anisotropy related to the spatial restriction of the local motion.

As pointed out by Burghardt and Thompson (1985), given that $\tau_1 > \tau_2$ and $\alpha_1 > \alpha_2$, only $r_1(t)$ will contribute to $r(t)$ at times longer than τ_1. The long rotational correlation time determined by anisotropy decay measurements, θ_l = 18 ns, corresponds to that of the whole protein, θ_p. This corroborates the steady-state anisotropy results suggesting that Trp in class 2 is very rigidly bound to the protein, i.e.

$$r_2(t) = r_0 e^{-t/\theta_p} \quad (11)$$

This leads to

$$r(t) = e^{-t/\theta_p}[r_0 + (r_0 - r_{\infty 1})\alpha_1 e^{-t/\tau_1}(e^{-t/\theta_{loc1}} - 1)/(\alpha_1 e^{-t/\tau_1} + \alpha_2 e^{-t/\tau_2})] \quad (12)$$

When $\tau_1 \gg \tau_2$ and $\alpha_1 > \alpha_2$, eq 12 becomes

$$r(t) = e^{-t/\theta_p}(r_{\infty 1} + (r_0 - r_{\infty 1})e^{-t/\theta_{loc1}}) \quad (13)$$

and the anisotropy decay is identical to that of species 1 alone.

In our case, $\tau_1/\tau_2 \simeq 4$. When $t < 2\tau_2$, we cannot rigorously neglect $\alpha_2 e^{-t/\tau_2}$ in front of $\alpha_1 e^{-t/\tau_1}$. However, when $t \geq 2\tau_2$, the anisotropy decay becomes similar to that of species 1:2.5

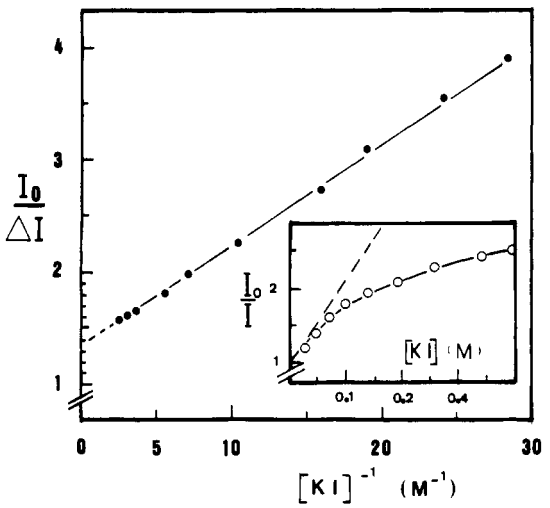

FIGURE 5: Iodide quenching of F75 TetR fluorescence intensity. In this modified Stern–Volmer plot, $I_0/(I_0 - I)$ is plotted as a function of the inverse of iodide concentration. The fluorescence intensity has been measured and corrected as described in Materials and Methods. Insert: Stern–Volmer plot of the quenching.

ns after the excitation, the ratio $\alpha_2 e^{-t/\tau_2}/\alpha_1 e^{-t/\tau_1}$ is around 0.1. At the precision of our measurements, the anisotropy decay of the protein gives an estimate for that of the long-lifetime species. In this case, the short rotational correlation time, θ_s, is such that

$$1/\theta_s \simeq 1/\theta_{loc1} + 1/\theta_p \simeq 1/\theta_{loc1} \qquad (14)$$

From the comparison of these parameters with those determined by steady-state anisotropy measurements, it can be inferred that tryptophans of class 2 are tightly stuck in their spatial environment, whereas those of class 1 exhibit substantial internal motion.

Iodide Quenching. The Stern–Volmer plot of the quenching of F75 TetR fluorescence by iodide was not linear but showed a marked downward curvature (Figure 5, inset). When only a part of the fluorescence emission is accessible to a diffusional quencher, the following modified Stern–Volmer equation can apply (Lehrer, 1971):

$$I_0/(I_0 - I) = 1/\alpha(1 + 1/K_{SV}[Q]) \qquad (15)$$

where I_0 is the fluorescence intensity in the absence of the quencher, I is the fluorescence intensity in the presence of the quencher at a concentration [Q], α is the fraction of the fluorescence intensity accessible to the quencher, and K_{SV} is the Stern–Volmer constant.

The modified Stern–Volmer plot of the quenching of F75 TetR by iodide was linear (Figure 5). The intersection of the extrapolated plot with the y axis corresponds to the inverse of the fraction of accessible chromophore, 0.7. The calculated apparent Stern–Volmer quenching constant (K_{SV} = 17.4 M^{-1} s^{-1}) is in good agreement with that previously observed (Hansen et al., 1987).

Iodide quenching was also monitored by lifetime measurements. The long lifetime was markedly quenched by iodide, whereas the short lifetime could not be quenched easily (Figure 6a). This strongly suggests that class 2 is not accessible to iodide. The accessible fraction of class 1 fluorescence could be determined from the modified Stern–Volmer plot of the long-lifetime component (Figure 6b). This fraction (0.8) and the weight of this class in the total fluorescence intensity (0.84) correlate well with the accessible fraction of the total fluorescence intensity (0.7), which seems to be almost entirely issued from the accessible fraction of class 1 fluorescence.

The analysis of the decay of Trp-43 at 0.2 M iodide is reported in Table II. τ_1 decreased by about 50%, while τ_2 was not significantly altered. The amplitudes associated with the two components and their correlation rotational times were not altered. The apparent radiative decay rate, determined as previously described, was not changed in the presence of iodide.

Denaturation by Guanidine Hydrochloride. Figure 7 reports the effects of progressive addition of guanidine hydrochloride on the steady-state fluorescence emission of F75 TetR. The fluorescence intensity decreased monotonically. In contrast, a biphasic effect was observed for the emission maximum. After an initial decrease in the emission maximum from 351 nm in the absence of GuCl to 342 nm in the presence of 1 M GuCl, the fluorescence spectrum of F75 TetR was progressively red-shifted to 352 nm in the presence of 6 M GuCl. This wavelength was similar to that observed for the emission maximum of Trp zwitterion in water, as determined on our experimental device.

Decay data also shed light on the differences in the behavior of Trp-43 in the presence of 1 M or 6 M GuCl. The analysis of the fluorescence decay at 350 nm is reported in Table II. The addition of 1 M GuCl induced a slight decrease in the

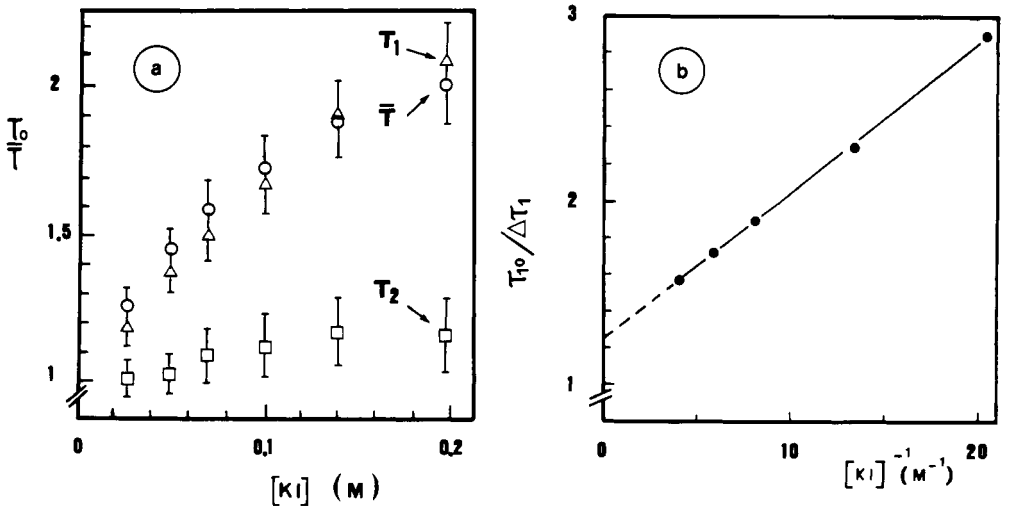

FIGURE 6: Iodide quenching of F75 TetR decay. (a) Stern–Volmer plot of the quenching of F75 TetR mean lifetime (circles), long lifetime (triangles), and short lifetime (squares). (b) Modified Stern–Volmer plot of the quenching by potassium iodide of the long lifetime. The emission wavelength was 345 nm.

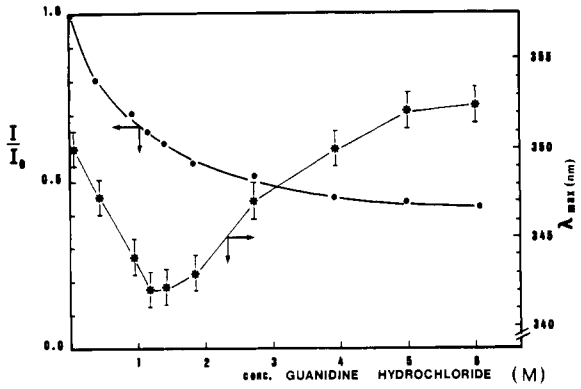

FIGURE 7: Effect of guanidine hydrochloride on the total steady-state fluorescence (circles) and maximum emission wavelength (asterisks) of F75 TetR.

weight of the long-lifetime component. At 6 M GuCl, the weight of the short-lifetime component further increased, whereas each lifetime decreased slightly. The decrease in the quantum yield in the presence of 1 M GuCl correlates well with the changes in the decay parameters (apparent radiative decay rate of Trp-43 0.035×10^9 s^{-1}) and the degree of static quenching is not significantly altered. The addition of 6 M GuCl induced a slight decrease in the apparent radiative decay rate of Trp-43 to 0.032×10^9 s^{-1}, which could be related to an increase in the static quenching due to the entire disruption of the protein structure. The observation that the degree of static quenching is not significantly altered in the presence of 1 M GuCl, whereas the relative amplitude of the two components is markedly changed, strongly suggests that the two components have a similar degree of static quenching.

The anisotropy increased slightly in the presence of 1 M GuCl (e.g., 0.12 at 350 nm, compared to 0.10) and then decreased markedly in the presence of 6 M GuCl (0.06 at 350 nm) (Figure 8a). The correlation rotational time of the long-lifetime species was not altered in the presence of 1 M GuCl, whereas that of the second component markedly decreased to 4 ns. At 6 M GuCl, θ_1 decreased to 1 ns and θ_2 further decreased to 0.7 ns, showing that the specific structure of the Trp-43 microenvironment was entirely destroyed under these conditions.

The anisotropy-associated spectra of F75 TetR have been calculated in the presence of 1 M GuCl (Figure 8b). The normalized AAS were not altered as compared with that of the native protein, but the relative weight of class 1 decreased, which is consistent with the fluorescence decay results. This shift of the equilibrium to the short-lifetime component can explain the blue shift observed in the fluorescence spectrum in the presence of 1 M GuCl. In the presence of 6 M GuCl, the low value of the fluorescence anisotropy prevented us from determining the AAS.

Iodide quenching experiments were also carried out in the presence of 1 or 6 M GuCl. The percent of accessible chromophore determined by the plot of $I_0/(I_0 - I)$ was 0.9 and 1.0 and appears as a clue for the deletion of the constraining environment structure of the short-lifetime component (class 2).

Salt Effect. Addition of KCl induced a decrease in the fluorescence intensity of F75 TetR up to 20% of the initial fluorescence intensity at 3 M KCl (Figure 9). Simultaneously, a slight blue shift in the emission maximum was observed: the emission maximum was 347 nm at 3 M KCl. A slight increase in the fluorescence anisotropy was also observed (Figure 10a). The analysis of the fluorescence decay at 3 M KCl is summarized in Table II. The lifetimes were not altered by salt

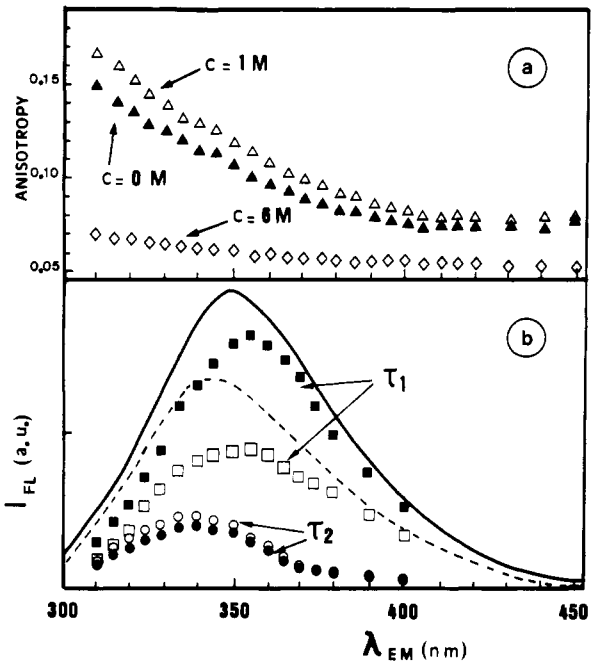

FIGURE 8: Effect of guanidine hydrochloride on the anisotropy of F75 TetR. (a) Steady-state fluorescence anisotropy of F75 TetR as a function of the emission wavelength at different concentrations of guanidine hydrochloride: 0 M (closed triangles), 1 M (open triangles), and 6 M (open diamonds). (b) Resolution of F75 TetR fluorescence emission spectrum into two spectra associated with the respective anisotropies of the two classes (class 1, squares; class 2, circles), in the absence (closed symbols, $r_1 = 0.07$, $r_2 = 0.25$) and in the presence of 1 M guanidine hydrochloride (open symbols, $r_1 = 0.07$, $r_2 = 0.20$). The solid line represents the steady-state fluorescence intensity of F75 TetR in the absence of guanidine hydrochloride, and the broken line represents that in the presence of 1 M guanidine hydrochloride.

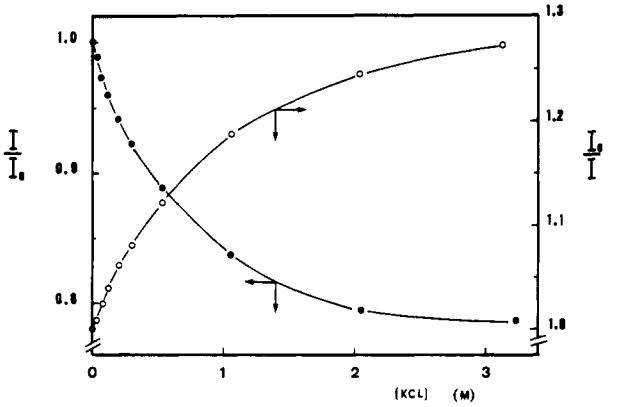

FIGURE 9: Effect of the concentration of potassium chloride on the steady-state fluorescence intensity of F75 TetR. The ratio I/I_0 is represented by the open circles, whereas I_0/I is represented by the closed circles.

addition, but the amplitude of the short-lifetime component increased, which is consistent with a shift of the equilibrium to the short-lifetime component. Analysis of the anisotropy showed that θ_1 was not altered, whereas θ_2 slightly decreased to 12 ns. The AAS were calculated and are shown in Figure 10b. The normalized anisotropy associated spectra were not altered. Their weights, however, have changed. That of the long-lifetime component decreased, in agreement with the shift observed by time-resolved fluorescence. The decrease in the intensity and the blue shift in the spectrum observed at high ionic strength can thus be explained by the decrease in the weight of the long-lifetime component. As observed in the presence of 1 M GuCl, the degree of static quenching was not significantly altered in the presence of 3 M KCl.

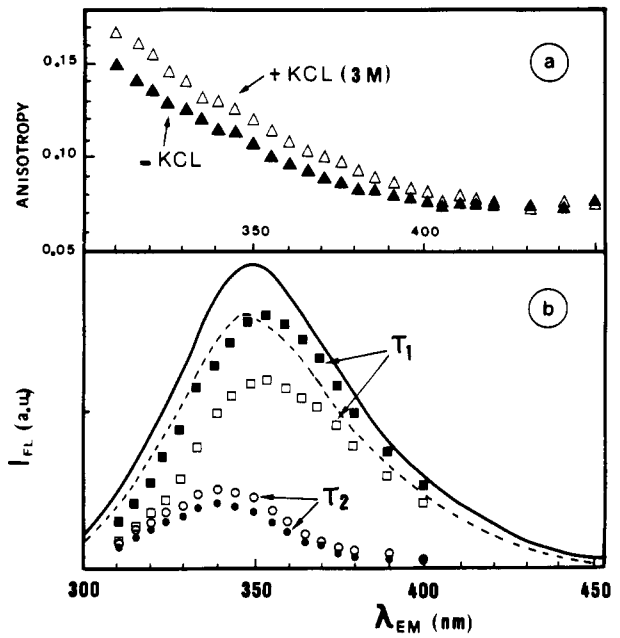

FIGURE 10: Effect of potassium chloride on the anisotropy of F75 TetR. (a) Steady-state fluorescence anisotropy of F75 TetR as a function of the emission wavelength in the absence (closed triangles) or in the presence of 3 M potassium chloride (open triangles). (b) Resolution of F75 TetR fluorescence emission spectrum into two spectra associated with the respective anisotropies of the two classes (class 1, squares; class 2, circles), in the absence (closed symbols, $r_1 = 0.07$, $r_2 = 0.25$) and in the presence (open symbols, $r_1 = 0.07$, $r_2 = 0.24$) of 1 M potassium chloride. The solid line represents the steady-state fluorescence intensity of F75 TetR in the absence of potassium chloride, and the broken line represents that in the presence of 1 M potassium chloride.

An explicative mechanism which may be invoked relies upon the thermodynamic properties of water in concentrated salt solutions. The hydrogen-bond network of the solvent water molecules is largely disrupted by ionic species, increasing the potential of hydrosolvation of hydrophobic areas (see Discussion).

Discussion

Origin of the Biexponential Decay of F75 TetR. The fluorescence decay of a chromophore is usually analyzed as functions that are sums of exponentials. In most cases, a limited number of discrete exponential components (<4) can give an adequate fit of the data. The physical meaning of these components has been widely discussed over the past years. Components with different lifetimes can be artifactually correlated in the analysis procedure (Badea & Brand, 1979; Demmer et al., 1987; Royer et al., 1990). Continuous or discrete distributions of exponentials (James & Ware, 1985; 1986; Alcala et al., 1987a) and nonexponential fluorescence decay functions (Beddard et al., 1980; Richert, 1985) have also been proposed to describe fluorescence decay data. In any case, mathematical analysis of fluorescence decay only yields an empirical description and does not prove the validity of a model.

The number of exponentials required to describe the fluorescence decay of the single tryptophan residue in a protein varies from one, e.g., azurin (Szabo et al., 1983) and bacteriophage Pfl DNA binding protein (Gruelich et al., 1985), to four, e.g., phospholipase A2 (Ludescher et al., 1985) and apocytochrome *c* (Vincent et al., 1988). The fluorescence decay of most single-tryptophan proteins, however, can be analyzed using bi- or triexponential functions (for a review, see Beechem & Brand, 1985). Continuous lifetime distributions can also adequately describe protein decay (Alcala et al., 1987b; Bismuto et al., 1988).

Scheme I

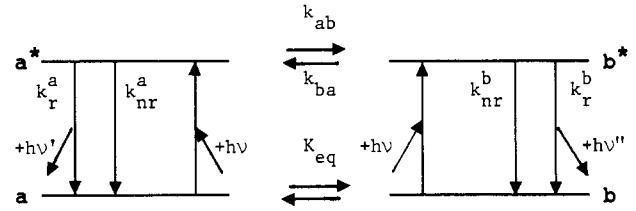

The conformer model (emission from different ground-state rotamers) is usually invoked to explain the biexponential decay of Trp zwitterion (Szabo & Rayner, 1980; Ross et al., 1981; Petrich et al., 1983; Gudgin-Templeton & Ware, 1984), although the nature of these conformers is controversial (Szabo & Rayner, 1980; Petrich et al., 1983). This model, however, must be extended to proteins with circumspection, as the nature of quencher groups in proteins is not clear. Alternative explanations for the multiexponential behavior of the fluorescence decay of Trp in proteins could be ground-state heterogeneities, excited-state reactions, or dipolar relaxation of the protein matrix around the excited state of the tryptophan residue. Different mechanisms of solvent relaxation have been proposed (for reviews see Simon, 1988; Maroncelli et al., 1989; Bagchi, 1989). Most of them are derived from dielectric continuum theory and imply a continuous red shift of the emission spectrum during the fluorescence lifetime. Molecular aspects of the solvent, however, could be important in understanding the mechanism of solvation (Karim et al., 1988).

Our experimental results clearly show that two decay times, independent of the emission wavelength, are sufficient to describe the fluorescence decay of F75 TetR throughout the spectrum. Moreover, the normalized time-resolved spectra of F75 TetR calculated as described elsewhere (Chabbert et al., 1989) display the existence of an isosbestic point around 345 nm (not shown). These results rule out dielectric continuum dipolar relaxation mechanisms. Moreover, the spectrum at time 0 extrapolated from our decay data (λ_{max} = 340 nm) is strongly red-shifted compared to that of a nondipolarly relaxed Trp in a protein [e.g., 327 nm for RNase T1, for which a vibronic structure is observable (James et al., 1985)]. This supports the assumption that the two emissive species observed are largely dipolarly relaxed.

Our decay data can be described by a general-two state model. In this model (Scheme I), two interconverting states, a and b, characterized by different decay rates, have a ground-state equilibrium constant of $K_{eq} = a_0/b_0$, whereas their excited states a* and b* interconvert with interconvertion rates k_{ab} and k_{ba}. The two decay times that describe the fluorescence decay of this system depend not only upon the individual intrinsic fluorescence lifetimes but also upon the rates of interconversion between the excited states (Donzel et al., 1974; Alcala et al., 1987b).

Whether the excited states interconvert during the excited-state lifetime cannot be resolved on the basis of existing decay data. Under the assumption that they do not interconvert ($k_{ab} = k_{ba} = 0$), the two states have been defined by a set of parameters: fluorescence lifetime, emission maximum, rotational correlation time, and quencher accessibility (see Results). The conspicuous convergence of the conclusions drawn from the evolution of these different parameters argues for the validity of this preliminary assumption. Taken together, the set of parameters that characterizes the two states strongly suggests that they correspond to two different local environments of Trp-43. This does not imply the existence of different

overall tertiary or quaternary protein conformations but implies that different Trp rotamers or local environments of this residue are included in the protein conformation.

The photophysical origin of a different lifetime for each state cannot be determined presently. In any case, it is probably more exact to relate the two associated states to classes or sets of conformations rather than to precise conformations, defined by tetrahedral angles. The existence of motions in proteins on time scales ranging from picosecond to nanosecond has been widely reported by experimental and theorical techniques such as nuclear magnetic resonance, X-ray diffraction, and molecular dynamics calculations (for review see McCammon and Karplus, 1983; Wuthrich & Wagner, 1984; Frauenfelder et al., 1988). The interconversion rates between the conformations accessible within a class would be much faster than the fluorescence decay time. In this case, a single fluorescence decay time corresponding to a combination of the lifetimes of the different conformations accessible would be observed (Donzel et al., 1974; Alcala et al., 1987b) and the behavior of the Trp within a class would be spectroscopically similar to that of a single conformational species.

Structural Properties of Trp-43 Environment. Tryptophan residues in the long-lifetime class (class 1) display a significant local motion (Table II). They have an emission spectrum very similar to that of Trp in water and are readily accessible by ionic quencher. This strongly suggests that this class is exposed to solvent. As illustrated in Table II, the negligible internal rotation of the Trp residues in the short-lifetime class (class 2) makes it obvious that these residues are very constrained. They could be either constrained in a protein environment or anchored on the protein surface by H-bonds. The former hypothesis is consistent with the blue-shifted fluorescence emission of these fluorophores and with their lack of accessibility to a fluorescence quencher.

According to available information concerning the helix–turn–helix motif, the intrinsic conformation of this motif as well as its orientation in relation to the rest of the molecule is fixed by a cluster of apolar residues, forming a hydrophobic core (for a review see Harrison & Aggarwal, 1990). Residues 15 and 18 in the conventional 20-residue-long α-helix–turn–α-helix motif are usually apolar and participate in the hydrophobic core holding the helix–turn–helix motif (reading head) in the right conformation to bind the operator. Trp-43 of TetR corresponds to residue 17 of the conventional helix–turn–helix motif (Postle et al., 1984). This residue is on the outside of the two-helix elbow and can be involved in sequence-specific DNA binding, e.g., Gln-33 in phage 434 repressor (Anderson et al., 1987; Aggarwal et al., 1988), Ala-49 in λ repressor, and Lys-32 in λ Cro (Hochschild et al., 1986). In the case of Trp repressor, the position of the homologous residue, Arg-84, depends on the presence or absence of tryptophan. In the presence of tryptophan, the side chain of Arg-84 interacts with the operator (Schevitz et al., 1985). In its absence, it collapses toward the hydrophobic core (Zhang et al., 1987). By analogy, we suggest that, for Trp-43 in TetR, an equilibrium could exist between residues exposed to solvent and residues embedded in this typical steric structure. Trp in class 2 would be specifically embedded, whereas Trp in class 1 would correspond to the residues exposed.

An additional evidence is given by the effects induced by disruptive agents such as high ionic concentration or moderate concentrations of guanidine hydrochloride. Alteration of hydrophobic interactions is expected to alter the hydrophobic core. Our results clearly show that the addition of disruptive agents such as high ionic strength or guanidine hydrochloride always induces two correlated effects: an increase in the amplitude of class 2 and a decrease in its rotational correlation time. Moreover, the larger the increase in the amplitude, the larger the decrease in the rotational correlation time. It is interesting to note that oxidation of TetR in the absence of DTT or β-mercaptoethanol induces a shift in the equilibrium similar to that induced by disruptive compounds (not shown). Disruptive compounds behave as solvation agents for hydrophobic regions in the protein and yield a more or less complete deletion of hydrophobic interactions stabilizing the native helix–turn–helix motif. Due to the partial removal of the steric hindrance on which its encagement depends, the entropy of Trp in class 2 is expected to increase and its free energy level to decrease. This should lead to a shift of the equilibrium to class 2 and a marked increase in the weight of this class, which is actually observed. Additionally, this kind of rationalization strongly suggests a metastable thermodynamic state to characterize the native α-helix–turn–α-helix motif which appears to be prone to disentangle.

Along with our definition of the two spectroscopic classes of Trp, it is interesting to point out the relevant role of the equilibrium between these two species as a valuable criterion for the evolution of the operator binding site conformation. Indeed, regardless of the decay properties of their excited states yielding a discrepancy in lifetimes, the components of classes 1 and 2 differ from each other in the steric hindrance they undergo in relation with their respective spatial microenvironments. This large congruence in spectroscopic properties and motional behavior has to be emphasized because it appears to be a pertinent way to describe the structural changes occurring in the α-helix–turn–α-helix motif and/or its environment and, subsequently, the functional properties of F75 TetR under various experimental conditions.

Investigation is currently in progress to explain temperature and tetracycline effects on the properties of F75 TetR. An analogous change of the Trp-43 environment is observed upon temperature increase but goes with side effects. In the case of tetracycline, the spectroscopic study is complicated by the occurrence of energy transfer from tryptophan to tetracycline. Nevertheless, preliminary results suggest that tetracycline binding similarly results in a destabilization of the operator binding site, which should be the key for allosteric regulation. These results will be the topics of further reports.

Finally, it turns out from this work that analysis of the fluorescence parameters of Trp-43 can provide relevant information on the structural properties of the operator binding domain of Tn10-encoded Tet repressor, on which its biological role depends.

Acknowledgments

We thank Dr. H. Lami for helpful discussions and advice, Mr. E. Piémont for expert assistance in data processing, Dr. Y. Boulanger for the amino acid analysis, Drs. A. Ross, M. Schnarr, and M. Granger-Schnarr for stimulating discussion, and Mrs. M. Wernert for editorial assistance.

Registry No. Trp, 73-22-3.

References

Aggarwal, A. K., Rodgers, D. W., Drottar, M., Ptashne, M., & Harrison, S. C. (1988) *Science 242*, 899–907.

Alcala, J. R., Gratton, E., & Prendergast, F. G. (1987a) *Biophys. J. 51*, 587–596.

Alcala, J. R., Gratton, E., & Prendergast, F. G. (1987b) *Biophys. J. 51*, 597–604.

Anderson, J. E., Ptashne, M., & Harrison, S. C. (1987) *Nature 326*, 846–852.

Badea, M. G., & Brand, L. (1979) *Methods Enzymol. 61*, 378–425.
Bagchi, B. (1989) *Annu. Rev. Phys. Chem. 40*, 115–141.
Beck, C. G., Mutzel, R., Barbe, J., & Muller, W. (1982) *J. Bacteriol. 150*, 633–642.
Beddard, G. S., Fleming, G. R., Porter, G., & Robbins, R. J. (1980) *Philos. Trans. R. Soc. London, A 298*, 321–334.
Beechem, J. M., & Brand, L. (1985) *Annu. Rev. Biochem. 54*, 43–71.
Bertrand, K. P., Postle, K., Wray, L. V., Jr., & Reznikoff, W. S. (1983) *Gene 23*, 149–156.
Bismuto, E., Gratton, E., & Irace, G. (1988) *Biochemistry 27*, 2132–2136.
Burghardt, T. P., & Thompson, N. L. (1985) *Biochemistry 24*, 3731–3735.
Chabbert, M., Kilhoffer, M. C., Watterson, D. M., Haiech, J., & Lami, H. (1989) *Biochemistry 28*, 6093–6098.
Chignell, D. A., & Gratzer, W. B. (1968) *J. Phys. Chem. 72*, 2934–2941.
Cross, A. J., & Fleming, G. R. (1984) *Biophys. J. 46*, 45–56.
Demmer, D. R., James, D. R., Steer, R. R., & Verral, R. E. (1987) *Photochem. Photobiol. 45*, 39–48.
Donzel, B., Gauduchon, P., & Wahl, Ph. (1974) *J. Am. Chem. Soc. 96*, 801–808.
Frauenfelder, H., Parak, F., & Young, R. D. (1988) *Annu. Rev. Biophys. Biophys. Chem. 17*, 451–479.
Greulich, K. O., Wijnaendts van Resandt, R. W., & Kneale, G. G. (1985) *Eur. Biophys. J. 11*, 195–201.
Gudgin-Templeton, E. F., & Ware, W. R. (1984) *J. Phys. Chem. 88*, 4626–2631.
Gunsalus, R. P., & Yanofsky, C. (1980) *Proc. Natl. Acad. Sci. U.S.A. 77*, 7117–7121.
Hansen, D., & Hillen, W. (1987) *J. Biol. Chem. 262*, 12269–12274.
Hansen, D., Altschmied, L., & Hillen, W. (1987) *J. Biol. Chem. 262*, 14030–14035.
Harrison, S. C., & Aggarwal, A. K. (1990) *Annu. Rev. Biochem. 59*, 933–969.
Hillen, W., Klock, G., Kaffenberger, I., Wray, L. V., & Reznikoff, W. S. (1982) *J. Biol. Chem. 257*, 6605–6613.
Hillen, W., Gatz, C., Altschmied, L., Schollmeier, K., & Meier, I. (1983) *J. Mol. Biol. 169*, 707–721.
Hillen, W., Schollmeier, K., & Gatz, C. (1984) *J. Mol. Biol. 172*, 185–201.
Hochschild, A., Douhan, J., III, & Ptashne, M. (1986) *Cell 47*, 807–816.
Isackson, P. J., & Bertrand, K. P. (1985) *Proc. Natl. Acad. Sci. U.S.A. 82*, 6226–6230.
James, D. R., & Ware, W. R. (1985) *Chem. Phys. Lett. 120*, 455–459.
James, D. R., & Ware, W. R. (1986) *Chem. Phys. Lett. 121*, 7–11.
James, D. R., Demmer, D. R., Steer, R. P., & Verrall, R. E. (1985) *Biochemistry 24*, 5517–5526.
Karim, O. A., Haymet, A. D. J., Banet, M. J., & Simon, J. D. (1988) *J. Phys. Chem. 92*, 3391–3394.
Kolber, Z. S., & Barkley, M. D. (1986) *Anal. Biochem. 152*, 6–21.
Lakowicz, J. R. (1983) in *Principles of Fluorescence Spectroscopy*, pp 111–153, Plenum Press, New York.
Lederer, H., Tovar, K., Gisela, B., May, R. P., Hillen, W., & Heumann, H. (1989) *EMBO J. 8*, 1257–1263.
Lehrer, S. S. (1971) *Biochemistry 10*, 3254–3263.
Lipari, G., & Szabo, A. (1980) *Biophys. J. 30*, 489–506.
Ludescher, R. D., Volwerk, J. J., de Haas, G. H., & Hudson, B. S. (1985) *Biochemistry 24*, 7240–7249.
Maroncelli, M., MacInnis, J., & Fleming, G. R. (1989) *Science 243*, 1674–1681.
McCammon, J. A., & Karplus, M. (1983) *Acc. Chem. Res. 16*, 187–193.
Meech, S. R., Phillips, D., & Lee, A. G. (1983) *Chem. Phys. 80*, 317–328.
Mendez, B., Tachibana, C., & Levy, S. B. (1980) *Plasmid 3*, 99–108.
Miller, J. H., & Reznikoff, W. S. (1980) in *The Operon*, Cold Spring Harbor Laboratory Press, Cold Spring Harbor, NY.
Montoro, T., Chabbert, M., Tyrzyk, J., & Lami, H. (1989) *J. Chem. Phys. 89*, 2712–2719.
Oehmichen, R., Klock, G., Altschmied, L., & Hillen, W. (1984) *EMBO J. 33*, 539–543.
Pabo, C. O., & Sauer, R. T. (1984) *Annu. Rev. Biochem. 53*, 293–321.
Petrich, J. W., Chang, M. C., McDonald, D. B., & Fleming, G. R. (1983) *J. Am. Chem. Soc. 105*, 3824–3832.
Pigault, C., & Gêrard, D. (1989) *Photochem. Photobiol. 50*, 23–28.
Postle, K., Nguyen, T. T., & Bertrand, K. P. (1984) *Nucleic Acids Res. 12*, 4849–4863.
Ricci, R. W. (1970) *Photochem. Photobiol. 12*, 67–75.
Richert, R. (1985) *Chem. Phys. Lett. 118*, 534–538.
Ross, J. B., Rousslang, K. W., & Brand, L. (1981) *Biochemistry 20*, 4361–4369.
Royer, C. A., Gardner, J. A., Beechem, J. M., Brochon, J. C., & Matthews, K. S. (1990) *Biophys. J. 48*, 363–378.
Schevitz, R. W., Otwinowski, Z., Joachimiak, A., Lawson, C. L., & Sigler, P. B. (1985) *Nature 317*, 782–786.
Shinitzky, M., & Goldman, R. (1967) *Eur. J. Biochem. 3*, 139–144.
Simon, J. D. (1988) *Acc. Chem. Res. 21*, 128–134.
Szabo, A. G., & Rayner, D. M. (1980) *J. Am. Chem. Soc. 102*, 554–563.
Szabo, A. G., Stepanik, T. M., Wayner, D. M., & Young, N. M. (1983) *Biophys. J. 41*, 233–244.
Tovar, K., Ernst, H., & Hillen, W. (1988) *Mol. Gen. Genet. 215*, 76–80.
Unger, B., Klock, G., & Hillen, W. (1984) *Nucleic Acids Res. 12*, 7693–7703.
Valeur, B., & Weber, G. (1977) *Photochem. Photobiol. 25*, 441–444.
Vincent, M., Brochon, J.-C., Merola, F., Jordi, W., & Gallay, J. (1988) *Biochemistry 27*, 8752–8761.
Werner, T. C., & Forster, L. S. (1979) *Photochem. Photobiol. 29*, 905–909.
Wuthrich, K., & Wagner, G. (1984) *Trends Biochem. Sci. 9*, 152–154.
Yang, H.-L., Zubay, G., & Levy, S. B. (1976) *Proc. Natl. Acad. Sci. U.S.A. 73*, 1509–1512.
Zhang, R.-G., Joachimiak, A., Lawson, C. L., Schevitz, R. W., Otwinowski, Z., & Sigler, P. B. (1987) *Nature 327*, 591–597.